Journal of Alloys and Compounds 514 (2012) 170–173

Contents lists available at SciVerse ScienceDirect

Journal of Alloys and Compounds

journal homepage: www.elsevier.com/locate/jallcom

Soft magnetic and microwave characteristics of amorphous FeCoBNi–Al_2O_3 films deposited by RF magnetron co-sputtering

Xuan Xiong, Zekun Feng*, Wenyi Ren, Huan Lin, Shuoqing Yan

Department of Electronic Science and Technology, Huazhong University of Science and Technology, 430074 Wuhan, Hubei, China

ARTICLE INFO

Article history:
Received 12 October 2011
Received in revised form 8 November 2011
Accepted 9 November 2011
Available online 17 November 2011

Keywords:
Amorphous film
Soft magnetic properties
Microwave permeability spectra
Electrical resistivity

ABSTRACT

A series of FeCoBNi–Al_2O_3 films were fabricated on glass and polymer substrates by means of RF magnetron co-sputtering. Firstly, the FeCoB films with Al_2O_3 addition were investigated. To further improve the microwave characteristics of the films, the effects of the Ni content on the soft magnetic properties and microwave characteristics of $(Fe_{40}Co_{40}B_{20})_{97-x}Ni_x$–$(Al_2O_3)_3$ films were studied. As a consequence $(Fe_{40}Co_{40}B_{20})_{97}$–$(Al_2O_3)_3$ films doped with 28.64 at.% of Ni exhibit excellent properties with high saturation magnetization ($4\pi M_s$) of 1.67 T, high resonant frequency (f_r) of 2.58 GHz, high electrical resistivity (ρ) of 235.85 μΩ cm and the real part of permeability is about 300, which is maintained up to 2 GHz. These results show that the presented films possesses potential in designing micro-magnetic devices design for Monolithic Microwave Integrated Circuit (MMIC).

1. Introduction

In recently years, the development of MMIC has led to a demand for further miniaturization and higher frequency operation of magnetic devices [1]. In order to meet those demands, the operating frequencies of soft magnetic films, which have been used in magnetic devices, such as integrated inductors, noise suppressors, transformers and magnetic sensors for miniaturization, were moved above gigahertz frequency [2–5]. For those GHz bands applications, resonance frequency (f_r), permeability (μ) and eddy current losses were the three key factors of soft magnetic films. According to Stoner–Wohlfarth theory, $\mu_s \approx \mu_1 = 4\pi M_s/H_k$, where μ_s, μ_1, $4\pi M_s$ and H_k represent static permeability, low-frequency permeability, saturation magnetization and in-plane-uniaxial anisotropy field respectively and the Kittel equation, $f_r = (\gamma/2\pi)(H_k \times 4\pi M_s)^{1/2}$, where γ represent gyromagnetic ratio with $\gamma = 1.76$ GHz/T, soft magnetic films are required to both high $4\pi M_s$ and an appropriate high H_k. In addition, high electrical resistivity (ρ) is also needed to suppress eddy current loss in the gigahertz range [6,7].

To find new soft films for gigahertz application, many works have been reported. FeCoB thin films exhibit good soft magnetic properties with a high f_r. However, FeCoB thin films have large magnetostriction, their magnetic properties are very sensitive to film stress [8,9]. FeCoNi thin films show low magnetostriction, high μ and high $4\pi M_s$, but FeCoNi thin films have low f_r [10,11]. Magnetic metal–insulator granular films (MIGF) such as FeCoB–N_xO_y (N_xO_y = SiO_2, Al_2O_3, etc.) show both good soft magnetic properties and high ρ, as their unique microstructure with dielectric amorphous phase were random embedded in nano-sized ferromagnetic particles [12–15].

In this paper, the influence of the Al_2O_3 addition to FeCoB was investigated and the $(FeCoB)_{97}(Al_2O_3)_3$ films exhibit good properties with $4\pi M_s$ value of 1.73 T, f_r value of 2.12 GHz, H_k value of 34 Oe and ρ value of 126.75 μΩ cm. In order to improve the microwave characteristics, a series of $(Fe_{40}Co_{40}B_{20})_{97-x}Ni_x$–$(Al_2O_3)_3$ films were fabricated and measured. The main goal of this study is to explore the effects of the Ni addition to FeCoB–Al_2O_3 system on the soft magnetic properties and microwave characteristics with variations of the Ni content.

2. Experimental

The FeCoB–Al_2O_3 and FeCoBNi–Al_2O_3 thin films were co-sputtered on glass (Corning Cat. No. 2875-25) and polymer by RF magnetron sputtering. Two separate targets were used for sputtering. One was the $Fe_{40}Co_{40}B_{20}$ target with several Ni chips fixed on the target surface. The other was the Al_2O_3 target. The background pressure was less than 7×10^{-5} Pa. The sputtering Ar gas pressure was 0.2–0.4 Pa and the distance from target to substrate was 115 mm. During sputtering, the substrates were rotated at 60 rpm. To induce an in-plane uniaxial anisotropy, an external static magnetic field (~100 Oe) was applied parallel to the film plane during deposition. By varying the content of Ni, a series of films were obtained to investigate the soft magnetic properties and microwave characteristics of FeCoBNi–Al_2O_3 thin films. The structure of the films was investigated by a SHIMADZU XRD-7000 X-ray diffraction (XRD). The morphology of the films was examined using an SEIKO SPA 400 Scanning Probe Microscopy (SPM) and JEOL JSM6700F field emission scanning electron microscope (FESEM). The composition of the films was measured by an Oxford Xmax-20 energy-dispersive X-ray spectrometer (EDS) attached to a TESCON

* Corresponding author. Tel.: +86 27 87542494; fax: +86 27 87542494.
E-mail address: fengzekun@mail.hust.edu.cn (Z. Feng).

0925-8388/$ – see front matter © 2011 Elsevier B.V. All rights reserved.
doi:10.1016/j.jallcom.2011.11.047

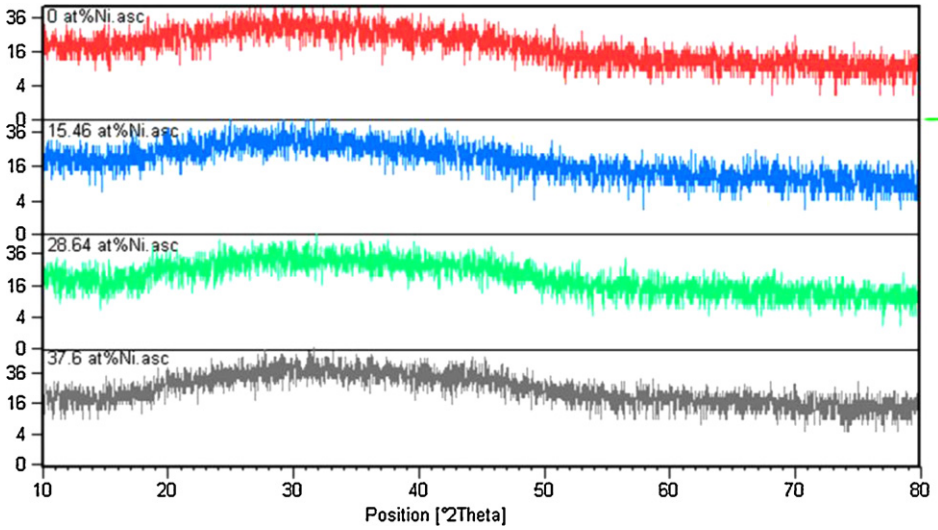

Fig. 1. The XRD patterns for the film of $x = 0$, 15.46, 28.64 and 37.6 at.%.

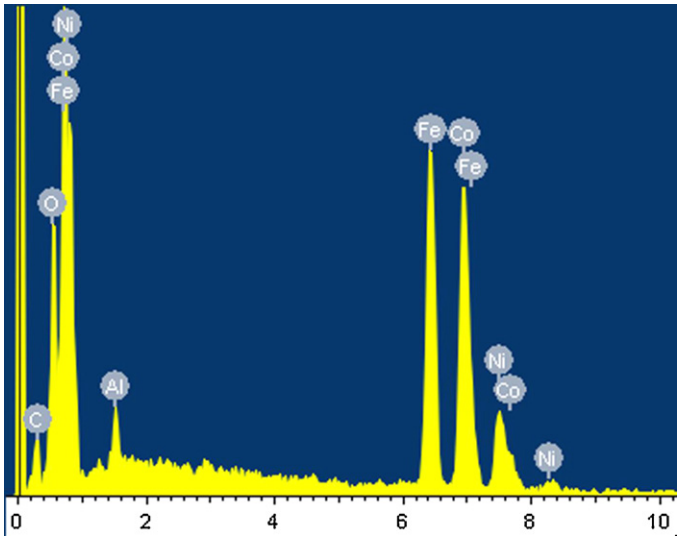

Fig. 2. EDS image of $(Fe_{40}Co_{40}B_{20})_{97-x}Ni_x$–$(Al_2O_3)_3$ films.

VEGA 3 environment scanning electron microscope (ESEM). The electrical resistivity was measured by the four-point probe method at room temperature. The static magnetic properties were measured with a Lakeshore 7407 vibrating sample magnetometer (VSM). The complex permeability spectra over the frequency range of 0.5–5 GHz was measured by the shorted microstrip transmission-line perturbation method with the use of 8722ES vector network analyzers.

3. Results and discussion

XRD patterns of the as-deposited $(Fe_{40}Co_{40}B_{20})_{97-x}Ni_x$–$(Al_2O_3)_3$ films were shown in Fig. 1. There were no evidences of diffraction peaks implying that the films exhibit an amorphous feature. This result indicated that Al_2O_3 was deposited as an amorphous phase and the structure of the films were not changed by Ni. From the EDS image of the films deposited on polymer substrates as shown in Fig. 2, the Al, O and Ni peaks could be seen that verified the Al_2O_3 and Ni by appending into FeCoB films.

The SPM image in Fig. 3 demonstrated that the surface of the films were very smooth and the root mean square roughness (Rms) was 4.047 nm. The cross-section microstructure of the films

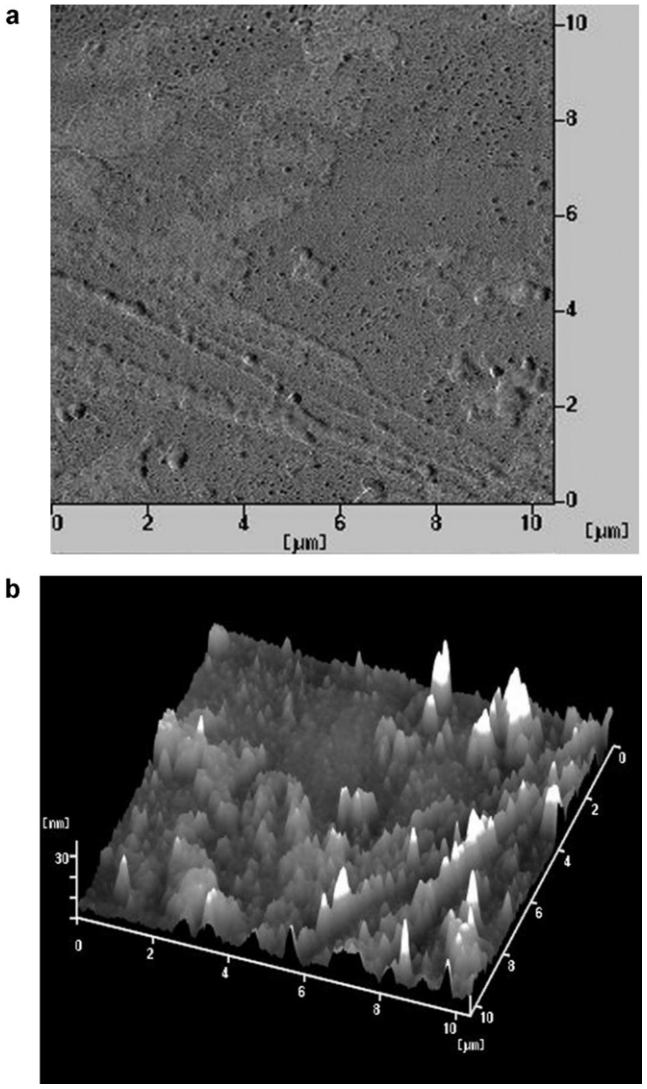

Fig. 3. SPM images of $(Fe_{40}Co_{40}B_{20})_{68.36}Ni_{28.64}$–$(Al_2O_3)_3$ thin film.

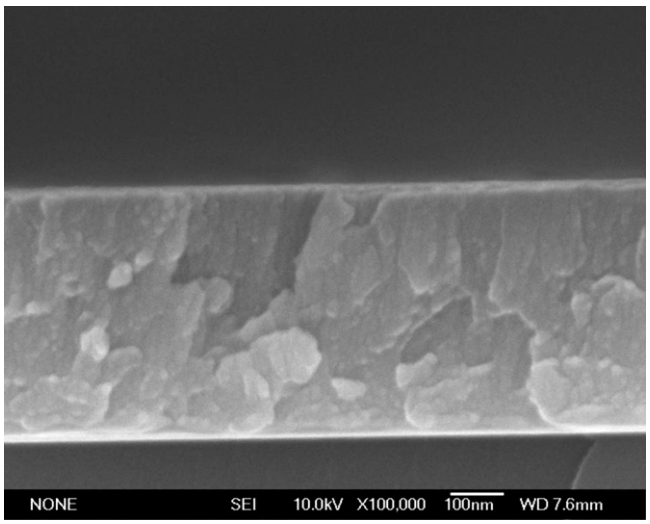

Fig. 4. FESEM images of $(Fe_{40}Co_{40}B_{20})_{68.36}Ni_{28.64}$–$(Al_2O_3)_3$ thin film.

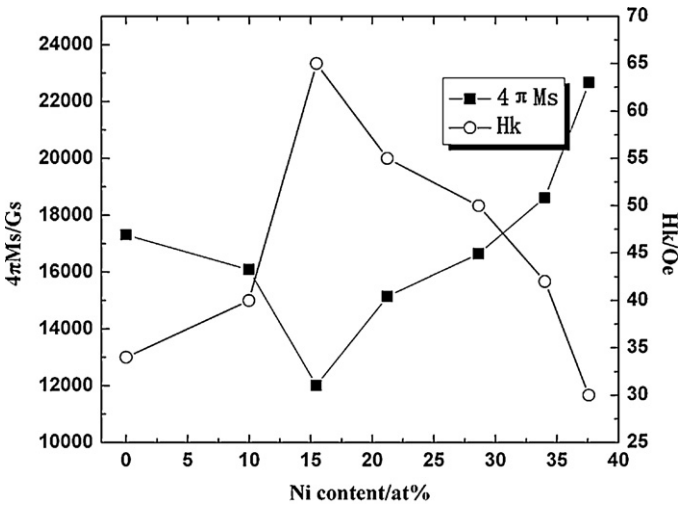

Fig. 6. $4\pi M_s$ and H_k as a function of Ni content.

was analyzed by FESEM (see Fig. 4), which clearly indicates that FeCoBNi–Al_2O_3 films were in amorphous state in consistence with the XRD patterns. The existence of an Al_2O_3 amorphous phase can prevent the effective crystal growth of Co–Fe alloy grains. The amorphous phase covering the Co–Fe alloy grains could probably suppress the diffusion of cobalt and iron ions [16].

As previously reported, the hard axis coercivity could be greatly decreased and the resistivity could be increased by an appropriate amount of Al_2O_3 [17]. By changing the input power of Al_2O_3 and FeCoB targets, many FeCoB–Al_2O_3 films have been fabricated with different Al_2O_3 ratios. With the lowest coercivity (H_c) and the highest saturation magnetization ($4\pi M_s$) in the above films, the $(FeCoB)_{97}(Al_2O_3)_3$ films showed good soft properties. The M–H loops along the easy and hard axes of the $(FeCoB)_{97}(Al_2O_3)_3$ films were measured as shown in Fig. 5.

To further improve the microwave characteristics, Ni was selected to add to the $(FeCoB)_{97}(Al_2O_3)_3$ films. Investigations on the effects of Ni addition have been done (see Figs. 6 and 7). Fig. 6 illustrates the $4\pi M_s$ and H_k of the as-deposited $(Fe_{40}Co_{40}B_{20})_{97-x}Ni_x$–$(Al_2O_3)_3$ films with different x. The Ni addition could remove the compressive residual stress from the films as a result of the segregation of B on the columnar boundaries [18].

So the saturation magnetization changes in the films might result from the three main aspects: (1) the decrease of the total FeCo content might reduce the saturation magnetization of the films, (2) the decrease of the B content and the increase of Ni content might enhance the saturation magnetization of the films, and (3) the extra coupling effect may form between different atoms, as the addition of Ni element can influence the position of the atoms in the films [15,19,20]. The $4\pi M_s$ initially decreases from 1.73 T for $x = 0$ to 1.20 T for $x = 15.46$ and then increases with further increase of x. Finally, the $4\pi M_s$ reach 2.27 T for $x = 37.6$. The H_k increases first and decreases afterwards with the increment of Ni content with the maximum values of 65 Oe. As shown in Fig. 7, f_r and H_c manifest a similar tendency, firstly increase and decrease monotonously afterwards, both with a maximum value at the same Ni content of 28.64 at.%. For the same Al_2O_3 volume, the H_c of the as-deposited films is related to the $4\pi M_s$, H_k and the average particle size. The similar variation tendency between the resonance frequency and coercivity could be interpreted by the above relation [14].

The frequency dependence of permeability of two typical films was shown in Fig. 8. From Figs. 5–8, magnetic properties and electrical resistivity of $(Fe_{40}Co_{40}B_{20})_{97-x}Ni_x$–$(Al_2O_3)_3$ thin films were concluded as show in Table 1.

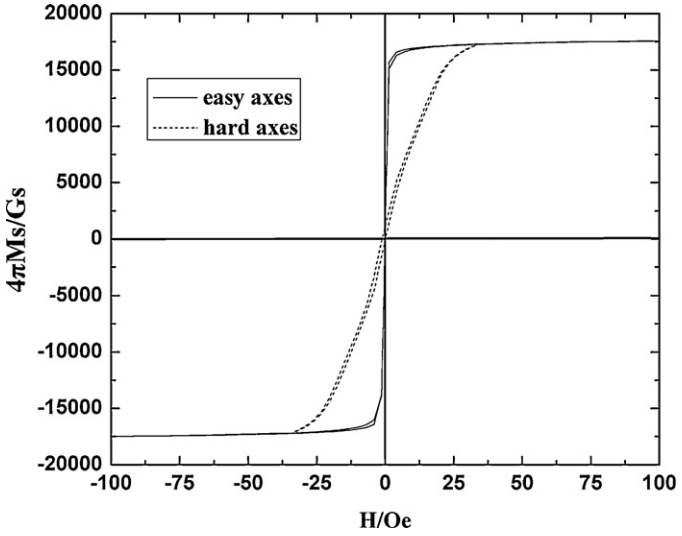

Fig. 5. The M–H loops along the easy and hard axes of the $(FeCoB)_{97}(Al_2O_3)_3$ film.

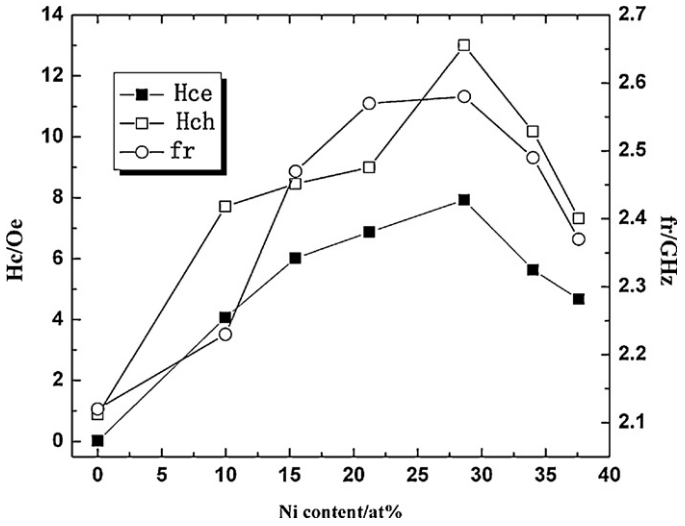

Fig. 7. f_r and H_c as a function of Ni content.

Table 1
Magnetic properties and electrical resistivity of $(Fe_{40}Co_{40}B_{20})_{97-x}Ni_x$–$(Al_2O_3)_3$ thin films: (a) without Ni dopant and (b) with 28.64 at.% of Ni.

Composition	$4\pi M_s$ (T)	H_{ch} (Oe)	H_{ce} (Oe)	H_k (Oe)	f_r (GHz) measured	f_r (GHz) calculated	ρ (μΩ cm)
(a)	1.73	0.01618	0.88017	34	2.12	2.05	126.75
(b)	1.67	7.9277	12.999	50	2.58	2.56	235.85

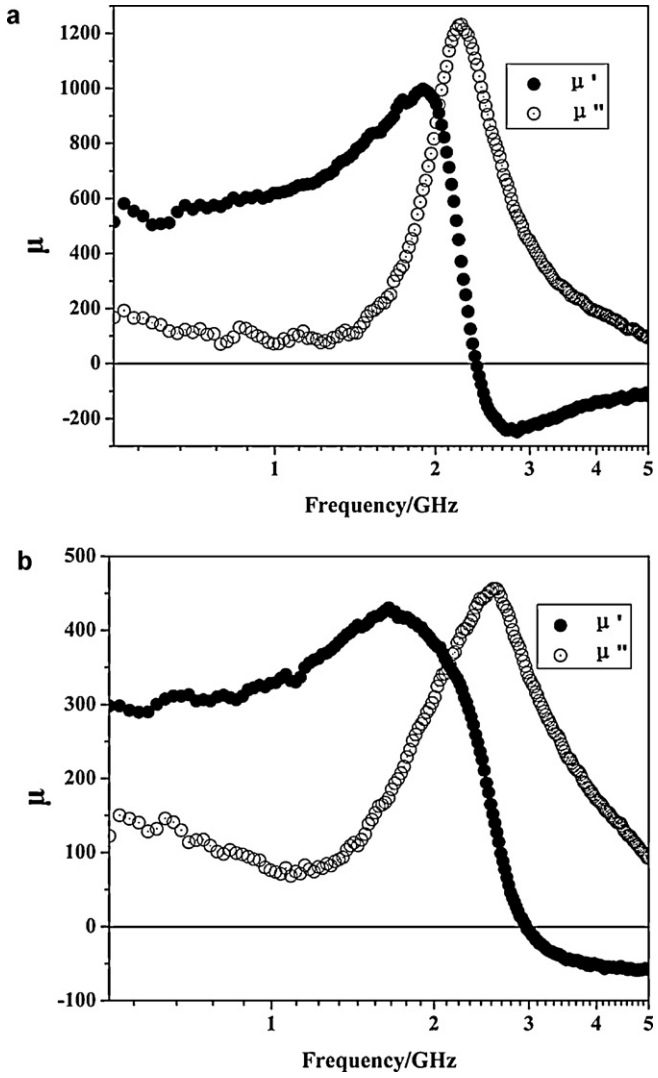

Fig. 8. Microwave permeability spectra of $(Fe_{40}Co_{40}B_{20})_{97-x}Ni_x$–$(Al_2O_3)_3$ film (a) $x = 0$ and (b) $x = 28.64$.

It is obvious that the H_k increases from 34 to 50 Oe and there was a corresponding increase in the f_r from 2.12 to 2.58 GHz by doping $(Fe_{40}Co_{40}B_{20})_{97}$–$(Al_2O_3)_3$ films with 28.64 at.% Ni. These results confirm the effectiveness of Ni addition to $(Fe_{40}Co_{40}B_{20})_{97}$–$(Al_2O_3)_3$ films on the microwave characteristics. According to Stoner–Wohlfarth theory and the Kittel equation, the f_r and μ_1 of the $(Fe_{40}Co_{40}B_{20})_{68.36}Ni_{28.64}$–$(Al_2O_3)_3$ films could be calculated of 2.56 GHz and 334, respectively. The experimental results were in good agreement with the expected values.

4. Conclusions

A series of FeCoBNi–Al_2O_3 films were fabricated with variation amount of $Al_2O_3$and Ni addition. By adjusting the input radio-frequency power of Al_2O_3 and FeCoB targets, the $(Fe_{40}Co_{40}B_{20})_{97}$–$(Al_2O_3)_3$ films were obtained with good soft properties. The influences of different Ni content on soft magnetic properties and microwave characteristics of as-deposited $(Fe_{40}Co_{40}B_{20})_{97-x}Ni_x$–$(Al_2O_3)_3$ films were also studied. The $(FeCoB)_{97}$–$(Al_2O_3)_3$ doped with 28.64 at.% of Ni exhibited high f_r of 2.58 GHz, high ρ of 235.85 μΩ cm and the real part of permeability is about 300, which is maintained up to 2 GHz. These results show that the presented films with large microwave permeability, high f_r and ρ have potential for the usage in the microwave devices for MMIC.

References

[1] S. Ohnuma, N. Kobayashi, T. Masumoto, et al., Journal of Applied Physics 85 (1999) 4574.
[2] M. Yamaguchi, K. Hyeon Kim, S. Ikedaa, Journal of Magnetism and Magnetic Materials 304 (2) (2006) 208–213.
[3] V. Bekker, K. Seemann, H. Leiste, et al., Journal of Magnetism and Magnetic Materials 290 (2005) 1434–1437.
[4] V. Korenivski, Journal of Magnetism and Magnetic Materials 215 (2000) 800–806.
[5] M. Xu, T.M. Liakopoulos, C.H. Ahn, IEEE Transactions on Magnetics 34 (4) (1998) 1369–1371.
[6] J.S. Liao, Z.K. Feng, J. Qiu, et al., Physica Status Solidi A 205 (12) (2008) 2943–2947.
[7] S.X. Wang, N.X. Sun, M. Yamaguchi, et al., Nature 407 (6801) (2000) 150–151.
[8] I. Kim, J. Kim, K. Him, et al., IEEE Transactions on Magnetics 40 (4) (2004) 2706–2708.
[9] C.L. Platt, M.K. Minor, T.J. Klemmer, IEEE Transactions on Magnetics 37 (4) (2001) 2302–2304.
[10] T. Osaka, M. Takai, K. Hayashi, et al., Nature 392 (6678) (1998) 796–798.
[11] Y.M. Kim, D. Choi, S.R. Kim, et al., Journal of Magnetism and Magnetic Materials 226 (2001) 1507–1509.
[12] M. Munakata, M. Yagi, M. Motoyama, et al., IEEE Transactions on Magnetics 37 (4) (2001) 2258–2260.
[13] J. Qiu, R.Z. Gong, Z.K. Feng, et al., Journal of Alloys and Compounds 496 (1–2) (2010) 467–471.
[14] S. Wang, X.D. Zhang, J.G. Li, et al., Applied Physics A: Materials Science & Processing 104 (1) (2011) 1–9.
[15] S. Wang, X.D. Zhang, J.G. Li, et al., Scripta Materialia 65 (1) (2011) 45–48.
[16] K. Ikeda, K. Kobayashi, M. Fujimoto, Journal of the American Ceramic Society 85 (1) (2002) 169–173.
[17] K. Shintaku, K. Yamakawa, K. Ouchi, Journal of Applied Physics 93 (2003) 6474.
[18] P. Zou, W. Yu, J. Bain, IEEE Transactions on Magnetics 38 (5) (2002) 3501–3520.
[19] E. Winkler, R.D. Zysler, M. Vasquez, et al., Physical Review B 72 (13) (2005) 132409.
[20] S. Ohnuma, H. Fujimori, S. Mitani, et al., Journal of Applied Physics 79 (8) (1996) 5130–5135.